Additive Manufacturing of Metallic Implants

Miguel Ribeiro Pinto
miguel.r.pinto@tecnico.ulisboa.pt
Instituto Superior Técnico, Universidade de Lisboa, Portugal
November 2021

Abstract

The number of bone fractures is increasing everyday, due to the increasing life expectancy and obesity spread in the world. The bone tissue engineering field has been developing temporary bone implants made of biodegradable metals, in which the application of iron lattice structures could be very promising. Only recent developments in the additive manufacturing technologies have also made possible the manufacturing of these structures. Hence, in the present work, a total of five unit cell topologies were analysed in order to find the topology with the closest mechanical properties to the trabecular bone. Numerical simulations were performed on every topology and the two unit cell topologies that revealed to have the engineering curves closer to the trabecular bone were chosen to be manufactured: cubic (C) and truncated cube (TC). These lattice structures were manufactured by L-PBF and later experimentally tested by means of compression testing, so that the numerical models could be assessed against the experimental results. The correlation between the numerical and experimental results required a careful analysis of the specimens obtained by L-PBF that revealed some geometric discrepancies between the initially designed structures. These discrepancies were identified and measured and the numerical models were revised accordingly. Finally, the numerical simulation results were compared with the experimental data and a good correlation was observed, validating the numerical models.

Keywords

Metallic implants; Lattice structures; Additive Manufacturing; Bone tissue engineering; Numerical analysis

1. Introduction

The number of bone fractures is increasing everyday due to a number of reasons, such as the continuous increase in life expectancy in the world and the spread of obesity [1]. According to the international osteoporosis foundation, more than 8.9 million bone fractures occur every year and, it is estimated that around 2050, hip fractures will have increased by 310% and 240% for men and women, respectively, when compared with rates of 1990 [1]. Due to this reason and the fact that when a bone fracture reaches a critical size, the body and the bone lose the ability to completely heal on its own [2], and medical treatment is required for a full recovery.

One of the most recent and emergent treatments that is now being used for bone regeneration, is bone tissue engineering (BTE), which applies principles of engineering and sciences to develop methods to synthesize and/or regenerate bones, such as the development of orthopaedic bone implants [3,4].

These are divided into two groups: permanent joint replacements and temporary fracture fixation devices. Currently, there is particular interest in the application of temporary bone implants in such a way that during the healing period they maintain their mechanical integrity, while progressively corroding and allowing to be replaced by the growing tissue, so that by the end of healing process the implant has been completely absorbed by the body [5].

Lattice structures are 3D cellular materials that show promising potential in the biomedical sector because of their permeable porous structures that, contrarily to fully dense (bulk) metallic implants, allow the flow of fluids through their structure, which can not only result in improved osseointegration, but also reduce stress shielding [6,7]. Currently, most of the research is focused on the development of biodegradable metal implants, due to their load-bearing properties [5].

The most studied biodegradable metals are magnesium (Mg), zinc (Zn) and iron (Fe) [8]. Out of these three, is the one with the highest mechanical properties and easiest to manufacture, although its degradation rate is too low [9].

The use of iron lattice structures in temporary bone implant applications could put together the best qualities of each: the porosity of lattice structures could not only accelerate the degradation rate of the iron, due to the increase in surface area, but also lower the mechanical properties of the iron to match those of bone, avoiding problems such as stress shielding, which is caused by an uneven load distribution across the bone due to the larger stiffness of the implant when compared to the bone [10,11].

The manufacturing of these type of structures in metal is not possible by any conventional method, due to their complexity [12]. Only recent developments in additive manufacturing (AM) techniques have made it possible [13], by technologies such as powder bed fusion (PBF).

The aim of this dissertation is to mechanically evaluate which iron open-celled lattice structure topology has the closest mechanical properties to the trabecular bone. For this, finite element analysis (FEA) and experimental compression tests were performed.

2. Methodology

The present work aims to find the unit cell topologies of lattice structures with the closest mechanical properties to those of bone for a given relative density, based on the polyhedrons chosen by Chantarapanich et al. [14] as the most suitable for tissue engineering. For this, finite element analyses (FEA) were performed, followed by experimental compression tests to assess the numerical model of the lattice structures.

2.1. Unit cell design

Six types of cellular structures were designed from different unit cells, which were selected based on the previous work of Chantarapanich et al. [14]. The open-celled lattice structures bring several advantages and are specially desirable in iron bone implant applications because the increased surface area could result in an increase in the degradation rate, so the five unit cell topologies selected are the most suitable open-celled polyhedrons: cubic (C), truncated cube (TC), truncated octahedron (TO), rhombicuboctahedron (RCO) and rhombi-truncated cuboctahedron (RTCO), presented in Figure 2.1.

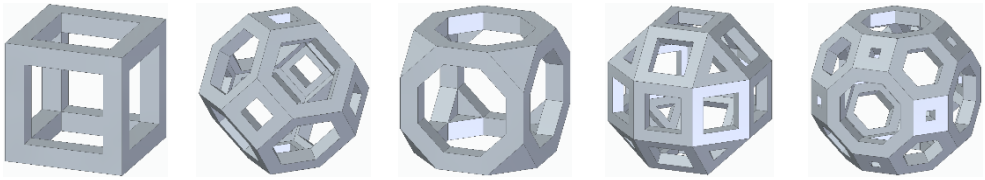

(a) (b) (c) (d) (e)

Figure 2.1 – Unit cells selected to be analysed: (a) cubic; (b) truncated octahedron; (c) truncated cube; (d) rombicuboctahedron; (e) rhombitruncated cuboctahedron

Each unit cell was designed to have a size of 3.5 x 3.5 x 3.5 mm^3, similar to Sharma et al. [9], so that the total size of the lattice structure would always be the same after replicating the unit cell as many times as wanted in each of the three directions, regardless of the topology. The design of the unit cells presented in Figure 2.1 was successfully performed using the CAD software Solid Edge 2020.

2.2. Numerical Modelling

The numerical simulations of the compression tests were performed using the software Siemens NX, version 1904. The program solver *Simcenter Nastran* uses the finite element method (FEM) to do the necessary calculations and the type of solution selected was the *SOL 106 Nonlinear Statics – Global Constraints*, which uses an implicit formulation that is applicable to static, quasi-static and nonlinear buckling analysis.

The yield criteria chosen was the von Mises yield criterion [15], and the boundary conditions considered for each simulation were a *simply supported constraint* at the base of the structure (Z=0), where the Z axis translation is fixed while all other 5 degrees of freedom are free, and an *enforced displacement constraint* on the top face of the lattice, which applies a set displacement value in the Z direction.

For the simulation of each lattice structure, a mesh refinement was performed so that reliable and accurate results were obtained. The convergence analysis considered the convergence of the effective stress, $\bar{\sigma}$ (von Mises stress) [15] for a given node of the mesh along the several refinements and the convergence of the reaction force response in the base of each lattice to the enforced displacement on the top face.

The material considered for the numerical simulations was pure iron (Fe), which is commercially available with 99.8% purity, from *Goodfellow Inc.*, Cambridge, UK. The mechanical properties of this material were previously assessed by Neves [16], and the Ludwik-Hollomon curve obtained and used in the numerical simulations is:

$$\bar{\sigma} = 984\bar{\varepsilon}^{0.229}\ MPa \tag{2.1}$$

To illustrate the convergence analysis, the topology C-0.57 (lattice structure that has cubic unit cells with a strut of 0.57 mm) was considered. This lattice structure consisted of 2 x 2 x 2 unit cells with a relative density of 25%. For these simulations, an enforced displacement of 1 mm, divided in 20 iterations of 0.05 mm each was imposed, corresponding to a total engineering strain of 14.29%.

The node in the successive generated meshes for this topology that was selected to obtain the effective stress value is shown in Figure 2.2 (a).

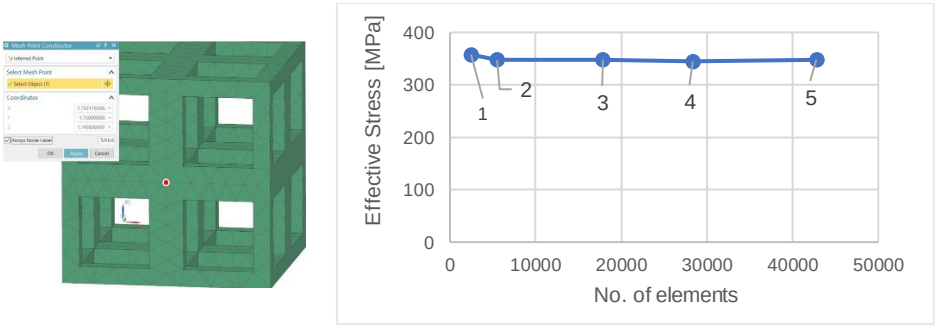

(a) (b)

Figure 2.2 – (a) Node 5866 selected to perform the convergence analysis on the effective stress, and (b) convergence analysis of the effective stress on node 5866 of C-0.57

In Figure 2.2 (b) is presented the convergence analysis of the effective stress. Figure 2.3, presents the force-displacement values considered for the convergence analysis of the reaction force response.

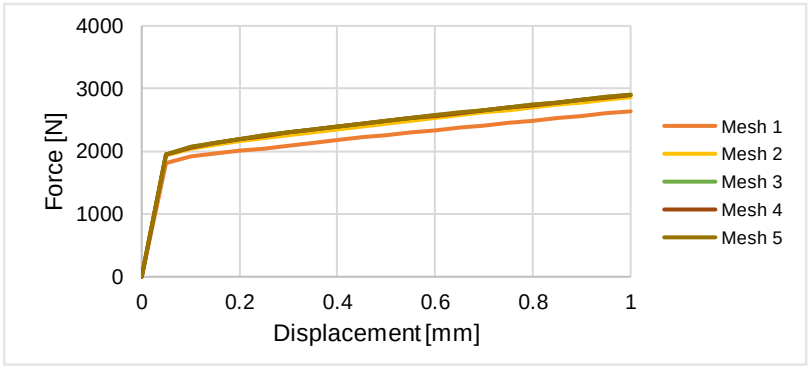

Figure 2.3 – Convergence analysis of the reaction force in the C-0.57 structure

After examining Figure 2.2 (b) and Figure 2.3 one can see that Mesh 3 can be chosen as representative of the structural reaction for this topology, as any further refinement does not bring any more accuracy. Most of the preliminary analyses were performed on a laptop equipped with an Intel i7-4710HQ CPU (2.5 GHz) and 12GB of RAM, while the topology analyses of the most complex structures and full models were performed on a desktop PC, equipped with an Intel i7-6950X CPU (3.0 GHz) and 128GB of RAM.

2.3. Relative density analysis

Initially, a relative density analysis was done to 3 cubic (C) lattice structures which consisted of 2 x 2 x 2 cells, with relative densities of 25%, 30% and 35%, to find the one with the closest mechanical properties to those of bone and decide on what will be the relative density for the remaining topologies. Table 2.1 summarizes the characteristics of the mesh of each topology and associated computation time that presented the best balance between accuracy and computational cost.

Table 2.1 – Comparison between each cubic topology

Topology	Element size [mm]	No. of elements	No. of nodes	Computation time
C-0.57	0.30	17850	34315	1min3s
C-0.64	0.30	20874	39173	2min51s
C-0.70	0.30	29056	52657	4min45s

The comparison between the engineering curves of each lattice structure with the corresponding relative density and the trabecular bone, for two values of apparent density, is shown in Figure 2.4.

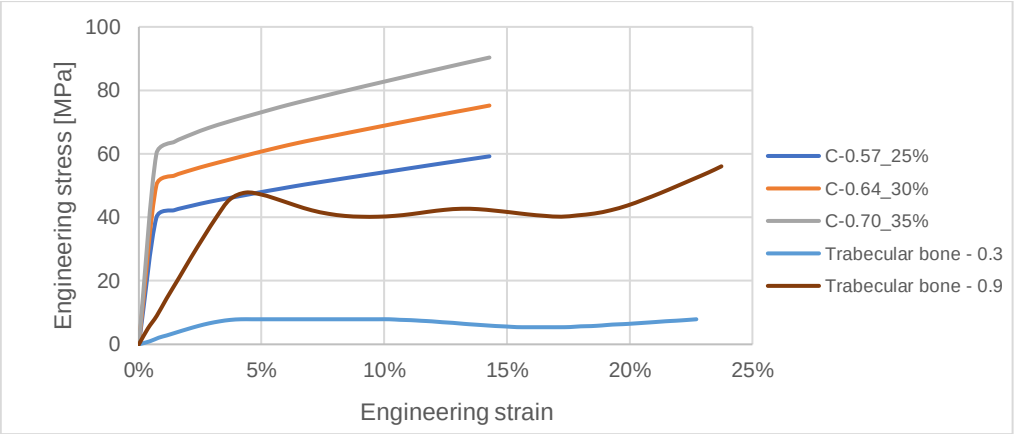

Figure 2.4 – Relative density analysis compared to trabecular bone properties

From the analysis of Figure 2.4, one can understand that the lattice structure that has the stress-strain values closest to any of the apparent densities of the trabecular bone is the C-0.57. For this reason, it was decided that every topology would have a relative density close to 25%.

2.4. Topology analysis

After defining 25% as the approximate relative density for every topology, a preliminary sensitivity analysis was done on every unit cell topology on smaller lattice structures, consisting of 2 x 2 x 2 cells and shown in Figure 2.5. These smaller scale analyses were performed so that the computational cost would be mitigated as much as possible, by trying to obtain the element size of the meshes that showed the best balance between accuracy of results and computational cost. This analysis will be extrapolated for the full models.

(a) (b) (c) (d) (e)

Figure 2.5 – Lattice structures 2 x 2 x 2: (a) C–0.57; (b) TC–0.50; (c) TO–0.33; (d) RCO–0.28; (e) RTCO–0.33

The unit cell parameters for each lattice structure and the characteristics of the meshes chosen for each topology and associated computation time are shown in Table 2.2, as well as the relative density and total model dimensions.

Table 2.2 – Unit cells and model characteristics for the preliminary topology analysis and mesh characteristics for each topology and computation solving times, (*) indicates solving times performed on the desktop PC

	Unit cell parameters		Model characteristics		Mesh characteristics			Computation time
Topology	Size (mm)	Strut (mm)	Total size (mm)	Relative density, ρ (%)	Element size (mm)	No. of elements	No. of nodes	
C–0.57		0.57		24.92	0.30	17850	34315	1min3s
TC–0.50		0.50		24.81	0.30	23345	44579	2min44s
TO–0.33	3.50	0.33	7.00	24.35	0.12	369922	575817	20min48s*
RCO–0.28		0.28		24.58	0.10	365052	622316	21min23s*
RTCO–0.33		0.33		25.32	0.08	667415	1090673	1h20min*

2.5. Experimental work

Experimental work was performed on the cubic (C) and truncated cube (TC) topologies, to validate the numerical models. The International Standard ISO 13314:2011 [17] was used for this purpose, as it is indicated for the mechanical testing of porous and cellular metallic materials with a porosity of 50% or more.

The specimens were manufactured by laser powder bed fusion (L-PBF) in the company Erofio, located in Marinha Grande, in a X Line 2000R from General Electrics [18]. The material available in the company Erofio for the manufacturing of the specimens was the 316 stainless steel. Due to this limitation, additional numerical simulations for this new material were also performed. The mechanical properties of the 316 stainless steel that were further considered for the numerical simulations were obtained from Kweon et al. [19].

Compression tests were performed at room temperature on the hydraulic testing machine *Instron SATEC 1200* that has a load cell of 1200 kN. The test was conducted at constant speed of 2.5 mm/min, following the standard ISO 13314:2011. Teflon sheets with a thickness of 0.5 mm were used to minimize friction between the specimen and the compression plates. Three specimens from each topology were compressed and a dry-run test was performed, without any specimen between the planes of the setup, to identify possible elastic deformation of the tool during the compression tests. After this procedure, it was possible to correct the displacement values in the mechanical curves.

3. Results and Discussion

The full models consist of 10 x 10 x 10 unit cells and the characteristics of these models are summarized in Table 3.1. The meshes generated to discretize the model of each topology were defined to have the selected element size.

Table 3.1 – Unit cells and model characteristics for the full model analysis

	Unit cell parameters		**Model characteristics**	
Topology	Size (mm)	Strut (mm)	Total size (mm)	Relative density, ρ (%)
C–0.57	3.50	0.57	35.00	24.92
TC–0.50		0.50		24.81
TO–0.33		0.33		24.35
RCO–0.28		0.28		24.58
RTCO–0.33		0.33		25.32

For these simulations, an enforced displacement of 5 mm was imposed, divided in 20 iterations of 0.25 mm, resulting in a total engineering strain of 14.29%.

3.1. Numerical analysis of the full models

The FEA of the full models revealed to have an excessive computational cost, and to perform the analyses, a simplification of the numerical model was needed. The solution found was to impose symmetry boundary conditions (BCs) where it was possible, so that there were less elements and nodes in the mesh, resulting in less computational time. To evaluate the feasibility of considering only a quarter of the numerical model in all the simulations, the C-0.57 topology was considered, and the numerical results for full, half and a quarter of the model were compared. Firstly, the full model of the lattice

structure, Figure 3.1 (a), was analysed, followed by only half (using one symmetry BC), Figure 3.1 (b), and, later, a quarter of the model (using both symmetry BCs), Figure 3.1 (c).

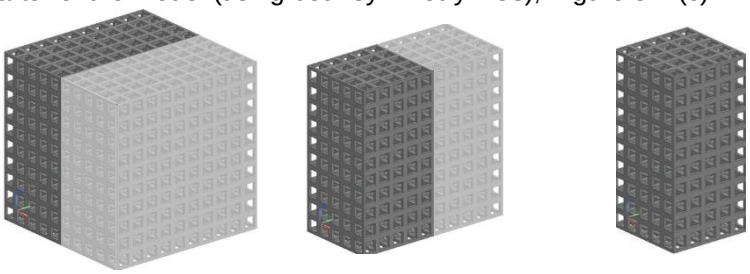

(a) (b) (c)

Figure 3.1 – Illustration of the C-0.57 structures analysed: (a) full model; (b) half model; (c) quarter of a model

The mesh generated for each of the numerical models was designed to have an element size of 0.3 mm. The force-displacement curves obtained for each model are completely overlapped, meaning that the results simulating a quarter of the model and imposing the symmetric constraints in the symmetry planes considered, allows to achieve very accurate results with significantly lower computational cost.

3.2. Numerical analysis of the topologies

The numerical results obtained in the simulations of the models from each topology are presented in this section and all simulations were performed in a quarter of the full model. The characteristics of the meshes and associated computation times of all topologies are presented in Table 3.2.

Table 3.2 – C-0.57, TC-0.50, TO-0.33, RCO-0.28 and RTCO-0.33 mesh characteristics and computation solving times, (*) indicates solving times of simulations performed on the desktop PC

Topology	Element size [mm]	No. of elements	No. of nodes	Computation time
C-0.57	0.3	545226	966687	55min24s*
TC-0.50	0.3	727983	1303171	1h29min*
TO-0.33	0.15	3747283	6807093	23h56min*
RCO-0.28	0.16	3839962	7168275	29h24min*
RTCO-0.33	0.15	2966889	5543400	22h1min*

An illustration of the results obtained for the effective strain of C-0.57, TC-0.50, TO-0.33, RCO-0.28 and RTCO-0.33 lattice structures is presented in Figure 3.2 (a), (b), (c), (d) and (e), respectively.

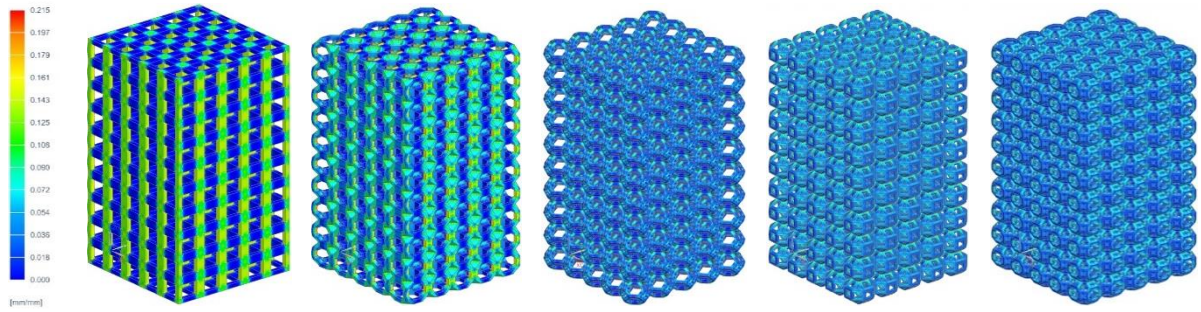

(a) (b) (c) (d) (e)

Figure 3.2 – Effective strain in the elements of the lattice structure: (a) C-0.57, (b) TC-0.50, (c) TO-0.33, (d) RCO-0.28 and (e) RTCO-0.33

The higher value of the maximum effective strain occurred for the RCO-0.28 lattice with a value of 0.215, and the lower value of the maximum effective strain occurred for the RTCO-0.33 lattice with a value of 0.147. The comparison between the engineering curves obtained from the numerical simulations for

each topology and the trabecular bone, for two different values of apparent density, is shown in Figure 3.3. And it is possible to observe that the C topology is the closest to the trabecular bone of 0.9 g/cm^3, the TO, RCO and RTCO topologies have their curves closer to the trabecular bone with an apparent density of 0.3 g/cm^3, however they do not reach the maximum engineering stress of the trabecular bone. The TC is positioned in between both curves of the trabecular bone.

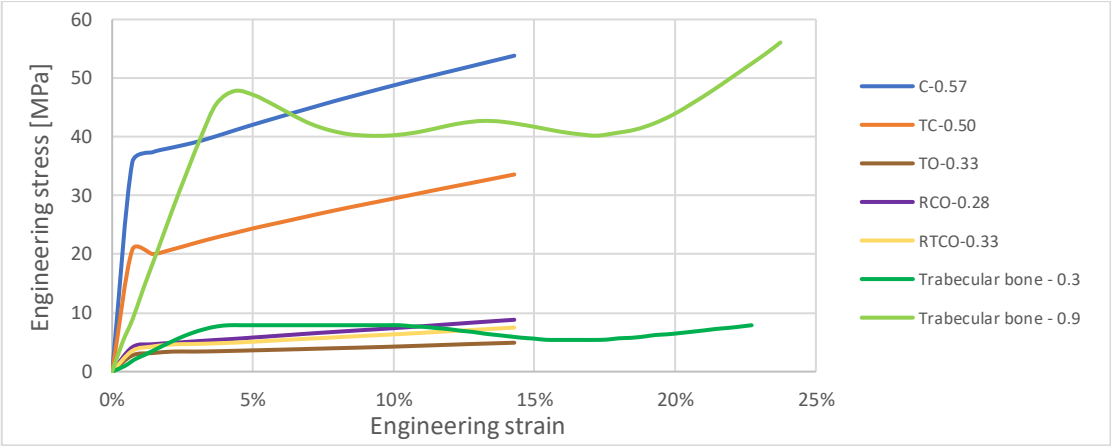

Figure 3.3 – Engineering curves from every topology compared to trabecular bone

For this reason, C and TC topologies were chosen to be experimentally tested. t_C

3.3. Experimental work results

As mentioned in section 2.5, six specimens in total were fabricated and tested. After taking a closer look at each specimen, some irregularities on the specimens' external surfaces were visible, such as burrs and sharp edges, see Figure 3.4 (a) and (b) respectively. For this reason, measurements of the external struts, of each specimen were taken using the measuring microscope TM-500 from Mitutoyo and the average strut size dimension found for each topology was 1.406 mm (C) and 1.198 mm (TC).

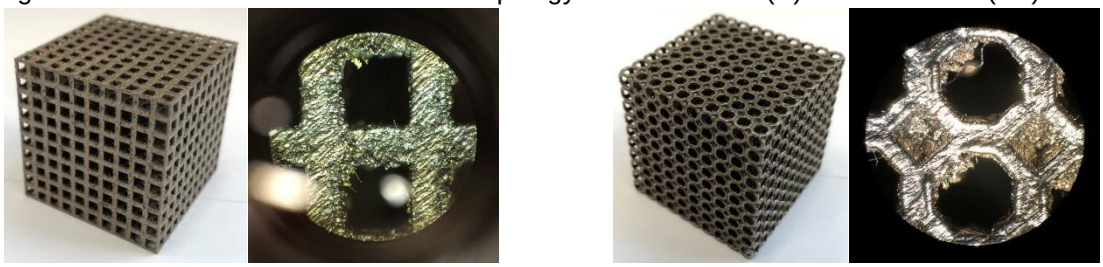

(a) (b)

Figure 3.4 – Specimens from the topologies selected: (a) cubic and (b) truncated cube

Figure 3.5 shows the compression specimens after being tested.

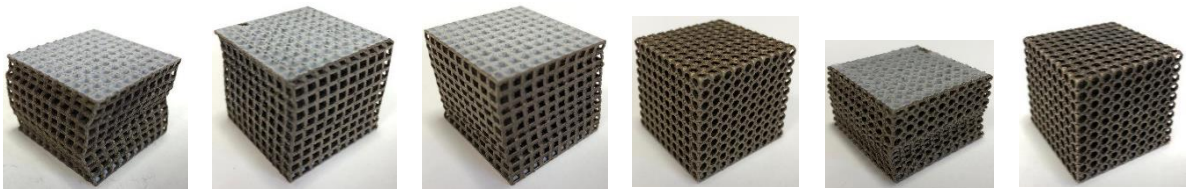

C1 Displacement 10.19 mm | C2 Displacement 4.92 mm | C3 Displacement 5.88 mm | TC1 Displacement 5.27 mm | TC2 Displacement 14.47 mm | TC3 Displacement 5.164 mm

Figure 3.5 – Compression test specimens after being tested and corresponding displacement performed

The engineering stress-strain curves obtained from the 3 specimens with the C topology and TC show a very good correlation.

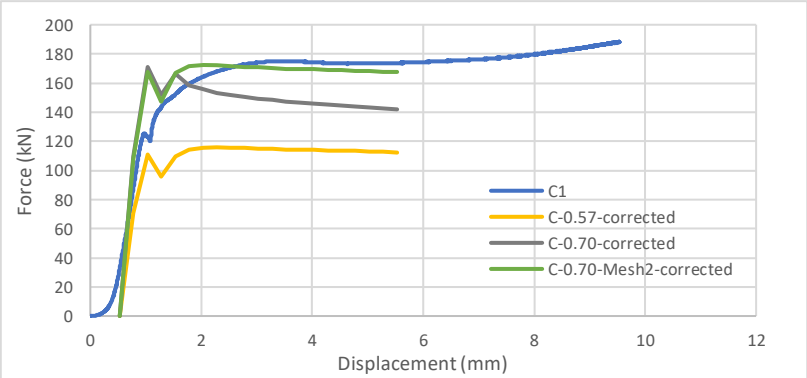

Figure 3.6 – Comparison between numerical and experimental results for cubic (C) topology

As can be seen from the inspection of Figure 3.6, the numerical results obtained for both meshes generated for the C-0.70 lattice structure showed a much better correlation to the experimental results when compared to the original designed C-0.57. The result obtained from refining the Mesh 1 and generating the Mesh 2, using the element size selected in section 2.4 for this topology, really brought the force-displacement numerical curve closer together to the experimental curve in the plastic regime, even replicating better its form.

4. Conclusions

The aim of this dissertation was to mechanically evaluate which iron open-celled lattice structure topology has the closest mechanical properties to the trabecular bone. For this, finite element analysis (FEA) and experimental compression tests were performed. The correlation between the numerical and experimental results required a careful analysis of the specimens obtained by L-PBF that revealed some geometric discrepancies against the initially designed structures. These discrepancies were identified and measured, and the numerical models were revised accordingly. Finally, the numerical simulation results were compared with the experimental data and a good correlation was observed, validating the numerical models.

References

[1] Prasad A. State of art review on bioabsorbable polymeric scaffolds for bone tissue engineering. Mater Today Proc [Internet]. 2021;44:1391–1400. Available from: https://doi.org/10.1016/j.matpr.2020.11.622.

[2] Crotty M, Badley EM. An international comparison of the estimated effect of the aging of the population on the major cause of disablement, musculoskeletal disorders. J Rheumatol. 1995;22:1934–1940.

[3] Roseti L, Parisi V, Petretta M, et al. Scaffolds for Bone Tissue Engineering : State of the art and new perspectives. Mater Sci Eng C [Internet]. 2017;78:1246–1262. Available from: http://dx.doi.org/10.1016/j.msec.2017.05.017.

[4] Bose S, Vahabzadeh S, Bandyopadhyay A. Bone tissue engineering using 3D printing. Mater Today [Internet]. 2013;16:496–504. Available from: http://dx.doi.org/10.1016/j.mattod.2013.11.017.

[5] Hermawan H. Updates on the research and development of absorbable metals for biomedical applications. Prog Biomater [Internet]. 2018;7:93–110. Available from:

https://doi.org/10.1007/s40204-018-0091-4.
[6] Arabnejad S, Johnston B, Tanzer M, et al. Fully Porous 3D Printed Titanium Femoral Stem to Reduce Stress-Shielding Following Total Hip Arthroplasty. 2017;29–31.
[7] Tan XP, Tan YJ, Chow CSL, et al. Metallic powder-bed based 3D printing of cellular scaffolds for orthopaedic implants : A state-of-the-art review on manufacturing , topological design , mechanical properties and biocompatibility. Mater Sci Eng C [Internet]. 2017;76:1328–1343. Available from: http://dx.doi.org/10.1016/j.msec.2017.02.094.
[8] Yusop AH, Bakir AA, Shaharom NA, et al. Porous Biodegradable Metals for Hard Tissue Scaffolds : A Review. Int J Biomater. 2012;2012.
[9] Sharma P, Pandey PM. Morphological and mechanical characterization of topologically ordered open cell porous iron foam fabricated using 3D printing and pressureless microwave sintering. Mater Des [Internet]. 2018;160:442–454. Available from: https://doi.org/10.1016/j.matdes.2018.09.029.
[10] Liverani E, Rogati G, Pagani S, et al. Mechanical interaction between additive-manufactured metal lattice structures and bone in compression: implications for stress shielding of orthopaedic implants. J Mech Behav Biomed Mater [Internet]. 2021;121:104608. Available from: https://doi.org/10.1016/j.jmbbm.2021.104608.
[11] Stress Shielding [Internet]. [cited 2021 Oct 6]. Available from: https://www.sciencedirect.com/topics/veterinary-science-and-veterinary-medicine/stress-shielding.
[12] Monteiro J. Design and Application of Lattice Structures on Sandwich Panels Core. Instituto Superior Técnico; 2019.
[13] Monteiro JG, Sardinha M, Alves F, et al. Evaluation of the effect of core lattice topology on the properties of sandwich panels produced by additive manufacturing. J Mater Des Appl. 2020;
[14] Chantarapanich N, Puttawibul P, Sucharitpwatskul S, et al. Scaffold library for tissue engineering: A geometric evaluation. Comput Math Methods Med. 2012;2012.
[15] Rodrigues J, Martins P. Tecnologia Mecânica - Tecnologia da Deformação Plástica (Vol I). 2nd ed. Escolar, editor. Portugal; 2010.
[16] Neves P. Finite element modelling of iron corrosion behavior. 2021;
[17] International Organization for Standardization. ISO 13314:2011 Mechanical testing of metals – Ductility testing – Compression test for porous and cellular metals (ISO Standard No. 13314:2011(E)). Int Organ Stand [Internet]. 2011;2011:1–7. Available from: www.iso.org.
[18] Additive G. Concept Laser X Line 2000R. 2021; Available from: https://www.ge.com/additive/additive-manufacturing/machines/x-line-2000r.
[19] Kweon H Do, Kim JW, Song O, et al. Determination of true stress-strain curve of type 304 and 316 stainless steels using a typical tensile test and finite element analysis. Nucl Eng Technol [Internet]. 2021;53:647–656. Available from: https://doi.org/10.1016/j.net.2020.07.014.